SI–HCCI Mode Transitions Without Open-Loop Sequence Scheduling: Online Parameter Adaptation

Patrick Gorzelic
Department of Mechanical Engineering,
University of Michigan,
Ann Arbor, MI 48109
e-mail: pgoz@umich.edu

Anna Stefanopoulou
Department of Mechanical Engineering,
University of Michigan,
Ann Arbor, MI 48109
e-mail: annastef@umich.edu

Jeff Sterniak
Robert Bosch LLC,
Farmington Hills, MI 48331
e-mail: jeff.sterniak@us.bosch.com

A parameter adaptation method for a previously developed spark ignition (SI) to homogeneous charge compression ignition (HCCI) combustion mode transition control architecture is described. The goal of the adaptive method is to use transient SI–HCCI transition data gathered in online operation to tune the controller model parameters on a cylinder individual basis, in order to improve the accuracy of the controller's model-based calculations and account for cylinder to cylinder variability and drifts over time. The parameter adaptation is implemented on an experimental engine in an indirect adaptive control structure where the model parameters of the SI–HCCI transition controller are updated based on real-time measurements and used in subsequent model-based calculations. Comparison of SI–HCCI transition responses before and after adaptation at a single operating condition shows notable benefits from use of the adaptive method. When tested at differing operating points, the performance of the adapted controller remains overwhelmingly favorable to that of the baseline controller even when conditioned on data from only a single operating point. [DOI: 10.1115/1.4036407]

1 Introduction

In a previous paper [1], a model-based feedback control architecture for spark ignition to homogeneous charge compression ignition (SI–HCCI) combustion mode transitions was developed. This control approach was shown to be capable of carrying out SI–HCCI transitions at multiple operating conditions while requiring calibration of only simple set points and controller gains. Such an approach offers advantages for generality and calibration simplicity relative to others in the literature [2–15]. These approaches employ open-loop scheduling of control input sequences either exclusively [2–11], or in a combined design that includes multiple open-loop trajectories accompanied by feedback elements [12–15]. For further discussion, see Ref. [1].

A major concern for model-based control performance is the accuracy of the model. This is especially important for SI–HCCI transitions, in which a large state and input transition occurs very quickly. There is thus limited time and measurements for direct output feedback control to compensate for errors, so that predictive model-based calculations play a major role. This is most obvious in the HCCI phase of the transition, where upon entry, no HCCI combustion feedback is yet available. The controller model of Ref. [1] was shown to fit a wide range of SI and HCCI data in Ref. [16]; however, accuracy may decrease as the engine ages and conditions are extrapolated outside those in the model parameterization. Additionally, cylinder to cylinder and engine to engine variability is not accounted for in the model parameterization.

This paper aims to improve the performance and robustness of the model-based control architecture of Ref. [1] by using transient SI–HCCI feedback to adaptively tune the combustion model parameters in an online parameter update scheme. The controller thus makes use of transient data not only for immediate corrective output feedback action, but also for improving model-based control calculations for successive transitions. In the paper, the adaptive methodology is described, and experimental examples are given, which show the effect of the parameter adaptation on the controller response.

2 Parameter Adaptation Method

2.1 Overview. The online parameter update method focuses on the combustion phasing and torque calculations of the model of Ref. [16], which play a central role in all of the nonlinear model-based calculations of the controller in Ref. [1] for both SI and HCCI mode (including the p_{im} reference derivation). The parameter update problems will be formulated in the linear parametric model framework where the model estimate $\widetilde{z}$ of the quantity z can be expressed as

$$\widetilde{z} = a^{\mathrm{T}}\Phi \tag{1}$$

where a is the parameter vector and Φ is the regressor vector. This allows standard linear parameter update laws to be used [17], which are easy to implement and favorable for real-time calculations.

All parameter update laws follow the recursive least squares with forgetting factor algorithm, which is chosen because of its desirable convergence and optimality properties [17]. The algorithm is reproduced here for convenience

$$a(m) = a(m-1) + G(m)(z(m) - \widetilde{z}(m)) \tag{2}$$

$$G(m) = P(m-1)\Phi(m)(\beta + \Phi^{\mathrm{T}}(m)P(m-1)\Phi(m))^{-1} \tag{3}$$

$$P(m) = (I - G(m)\Phi^{\mathrm{T}}(m))P(m-1)/\beta \tag{4}$$

where m is the update time index, $P = (\sum_{i=1}^{m} \Phi(m)\Phi^{\mathrm{T}}(m))^{-1}$ and β is a forgetting factor that discounts older data from q updates prior by a factor of q^{β}. The basis function matrix P of the recursive least squares algorithm is initialized at $10^{-3}I$ for torque adaptation laws and $10^{-2}I$ for combustion phasing adaptation laws, where these values were tuned in simulation to give some but not too much sensitivity in the first several parameter updates. The

Contributed by the Dynamic Systems Division of ASME for publication in the Journal of Dynamic Systems, Measurement, and Control. Manuscript received September 29, 2015; final manuscript received February 16, 2017; published online June 1, 2017. Assoc. Editor: Junmin Wang.

combustion phasing update laws are implemented using normalized regressor variables of the form

$$n_x = \frac{x - x_{\min}}{x_{\max} - x_{\min}} \tag{5}$$

that vary from 0 to 1 as the physical variable x varies between some reasonable maximum and minimum values. This was done for combustion phasing but not torque update laws because the combustion phasing models involve more variables with a wider span of units, as will be seen.

When the SI–HCCI transition commences, parameter updates are executed after feedback is obtained from each subsequent cycle. The adaptation is turned off after a certain number of cycles elapse in the HCCI phase, chosen to be ten for all cases. After each update, the new parameters are used immediately in the following cycle's model-based control calculations, creating an indirect adaptive control structure. Note that for all control loops in the architecture of Ref. [1], the model predicted quantity $\tilde{z}$ that is necessary for parameter updating is straightforward to generate from its corresponding model inverse calculation by simply running the calculation forward with the solved control input.

2.2 Spark Ignition Model Adaptation

2.2.1 Torque Model. The torque model adaptation focuses on the model's net mean effective pressure (NMEP) prediction. Because the NMEP calculation in the SI model of Ref. [16] is largely based on the simplified physics of polytropic compression and expansion work, it is difficult to devise a way to adapt the NMEP estimate directly. Its physicality implies that it contains few parameters that can be updated based on empirical data, and it is difficult to introduce new empirical parameters that provide sufficient sensitivity yet do not distort the various physical dependencies of the NMEP function and lead to unrealistic predictions in some conditions. For this reason, the NMEP adaptation is carried out by introducing an error term $\Delta_{\tau,S}$ between the baseline NMEP prediction NMEP^{mod} and the measured NMEP, which does not modify the baseline prediction. This error is then parameterized and estimated based on important influencing variables for the engine torque and the estimated value is added to the baseline NMEP calculation to form the final prediction, $\widetilde{\text{NMEP}}$

$$\Delta_{\tau,S} = \text{NMEP} - \widetilde{\text{NMEP}} \tag{6}$$

$$\widetilde{\text{NMEP}} = \text{NMEP}^{\text{mod}} + \widetilde{\Delta}_{\tau,S} \tag{7}$$

$$\widetilde{\Delta}_{\tau,S} = a_{\tau,S}^{\text{T}} \Phi_{\tau,S} \tag{8}$$

$$\Phi_{\tau,S} = [\, m_f \quad V_{\text{cmb}}^2 \quad V_{\text{cmb}} \quad 1 \,]^{\text{T}} \tag{9}$$

where $\Delta_{\tau,S}$ and $\widetilde{\Delta}_{\tau,S}$ are the actual and predicted errors in the SI NMEP calculation, m_f is the mass of fuel, and V_{cmb} is the combustion chamber volume at instantaneous combustion. The parameterization for the estimated prediction error $\widetilde{\Delta}_{\tau,S}$ is based on the fact the torque is normally a strong function of fuel quantity, and rolls off with a nonlinearly increasing slope as combustion departs from max brake torque (MBT) timing. The variable $V_{\text{cmb}} = V(|\theta_{50} - \theta_{50}^{\text{MBT}}|)$ where θ_{50} is the 50% mass fraction burned angle and V is evaluated with the crank slider equation [18]. V_{cmb} is meant to capture the nonlinear dependence of torque on combustion phasing based on the logic in Ref. [19] and is expressed in units of $dm^3 \times 10$. The V_{cmb} terms are included mostly for disambiguation in the SI–HCCI controller, so that in the event that a θ_{50} far from MBT occurs the controller can detect a torque reduction due to nonideal combustion phasing, rather than incorrectly attributing the effect to fuel quantity. The V_{cmb} terms will become more important for control in the HCCI to SI direction, which will be covered in a future paper.

A limitation of the adaptive parameterization in Eqs. (7)–(9) is that it assumes that the NMEP prediction error can be captured by additive terms. If a different error functional dependence such as multiplicative or exponential is present, the approximation of this error with additive terms will be weaker than if the true dependence were included. However, for the experiments in this paper, the simple additive adaptive parameterization was found to produce notable improvements in torque response, and so was retained for simplicity. Modification of the torque adaptation for more sophisticated adaptive parameterizations is an open topic for future work.

2.2.2 Combustion Phasing Model. The SI combustion phasing model is adapted by direct update of the SI θ_{50} correlation of the model of Ref. [1]

$$\widetilde{\theta}_{50} = a_{50}^{\text{T}} \Phi_{50} \tag{10}$$

$$\Phi_{50} = [n_f \;\; n_{\text{sp}}^2 \;\; n_{\text{sp}} \;\; n_{\text{evc}}^2 \;\; n_{\text{evc}} \;\; n_{\lambda'}^2 \;\; n_{\lambda'} \;\; 1]^{\text{T}} \tag{11}$$

$$n_f = \frac{m_f - 5}{20 - 5}, \quad n_{\text{sp}} = \frac{\theta_{\text{sp}} - (-60)}{0 - (-60)} \tag{12}$$

$$n_{\text{evc}} = \frac{\theta_{\text{evc}} - (-50)}{15 - (-50)}, \quad n_{\lambda'} = \frac{\lambda' - 1}{2 - 1} \tag{13}$$

where θ_{sp} is the spark timing, θ_{evc} is the EVC timing, and $\lambda' = 1/\phi' = (m_a + m_r)/\text{AFR}_s m_f$ characterizes the total dilution in the cylinder with m_a and m_r being the mass of air and residual and AFR_s being the stoichiometric air–fuel ratio (AFR). The maximum and minimum normalization limits are chosen based on the feasible range of the corresponding variable in the SI phase of the transition.

2.3 Homogeneous Charge Compression Ignition Model Adaptation

2.3.1 Residual Gas Temperature Correction: First HCCI Cycle. Based on the inspection in Ref. [16], any error in the combustion phasing prediction on the first HCCI cycle of the transition is attributed to the model's in-cylinder temperature prediction. Following the convention in Ref. [1], the first HCCI cycle will be referred to as *HCCI 0* and the final SI cycle will be referred to as *SI -1*. Cycle *HCCI 0* is thus distinct from the remainder of the HCCI cycles, where combustion phasing error will be attributed directly to error in the Arrhenius combustion phasing correlation. This policy is chosen following the results of Ref. [16], which suggest that the strongest source of error on cycle *HCCI 0* is in the excursion of the thermodynamic state far outside the nominal HCCI range, while for the remainder of the cycles it is mostly due to nominal model error. The combustion phasing error on cycle *HCCI 0* is captured by the residual gas temperature correction factor k_r introduced in Ref. [16], and the same method is applied to backtrack from the measured θ_{50} to the necessary k_r value for the parameter adaptation. The Arrhenius integral inversion involved in this method is carried out using the Arrhenius tabulation explained in Ref. [1], which allows execution in real-time. The details of the method are covered in Ref. [16] and so are not reviewed here. For the range of conditions examined, k_r is parameterized as a linear function of θ_{evc} as in Ref. [16]

$$\widetilde{k}_r = a_{k_r}^{\text{T}} \Phi_{k_r} \tag{14}$$

$$\Phi_{k_r} = [\, \theta_{\text{evc}} \quad 1 \,]^{\text{T}} \tag{15}$$

Note that on cycle *HCCI 0*, no parameter updates are executed other than the residual temperature correction, and on all cycles following the residual temperature correction update is deactivated.

2.3.2 Torque Model. Similar to the SI case, the HCCI NMEP calculation in the model of Ref. [16] comes mainly from simplified physics, with the exception of the combined thermal/

combustion efficiency factor η_λ. However, this factor is not convenient for use in adapting the torque model to match transient data, because it only accounts for the dependency of NMEP on AFR. Thus, the adaptation of the HCCI torque model is carried out following the same approach as in the SI case, where corrective parameters are introduced to account for error in the NMEP prediction

$$\widetilde{\text{NMEP}} = \text{NMEP}^{\text{mod}} + \widetilde{\Delta}_{\tau,H} \tag{16}$$

$$\widetilde{\Delta}_{\tau,H} = a_{\tau,H}^{\text{T}} \Phi_{\tau,H} \tag{17}$$

$$\Phi_{\tau,S} = [\, m_f \quad 1 \,]^{\text{T}} \tag{18}$$

where $\Delta_{\tau,H}$ and $\widetilde{\Delta}_{\tau,H}$ are the actual and predicted errors in the HCCI NMEP prediction, defined in the same manner as in Eq. (6). The dependence of the torque error is simplified to be a function of fuel only, because combustion phasing is typically constrained to a smaller window in HCCI than SI and so deviations of θ_{50} from the optimal cannot be as large. As is apparent from the SI–HCCI transitions of Ref. [1], the validity of this simplification can weaken on the first several HCCI cycles of the transition due to early combustion phasing caused by high exhaust temperatures. However, the torque model is not updated on the first HCCI cycle *HCCI 0* where only the k_r adaptation executes, which is often the point of earliest combustion phasing. A few early cycles may follow *HCCI 0*, that may not be captured properly with the simplified $\widetilde{\Delta}_{\tau,H}$ parameterization; however, the simplified parameterization still proved very helpful.

2.3.3 Combustion Phasing Model. As previously stated, error in the HCCI combustion phasing model on all cycles other than *HCCI 0* is attributed to the model's Arrhenius correlation. This correlation is given in Ref. [1] and is not straightforward to work with for developing a linear parameter update method, since the integrated Arrhenius rate creates a nonlinear and implicit function. However, it can be noted that many of the dependencies in the Arrhenius correlation are parameterized into the Arrhenius threshold K_{th}, which is an explicit expression that is linear in the parameters. The combustion phasing model update is thus carried out targeting the parameters of the Arrhenius threshold, while leaving the parameters n_p and E_a unchanged. A term to capture variation of in-cylinder temperature is augmented to the Arrhenius threshold, since the dependence of the Arrhenius correlation on in-cylinder temperature enters through the Arrhenius integral and so is inaccessible

$$K_{\text{th}}^* = \int_{\theta_{\text{ivc}}}^{\theta_{\text{soc}}^*} \frac{1}{\omega} p_c(\theta)^{n_p} e^{\left(\frac{-Ea}{RT_c(\theta)}\right)} d\theta \tag{19}$$

$$\theta_{\text{soc}}^* = (\theta_{50} - a_{\text{soc},0})/a_{\text{soc},1} \tag{20}$$

$$p_c(\theta) = p_{\text{ivc}} \left(\frac{V_{\text{ivc}}}{V(\theta)}\right)^{n_c}, \quad T_c(\theta) = T_{\text{ivc}} \left(\frac{V_{\text{ivc}}}{V(\theta)}\right)^{n_c - 1} \tag{21}$$

$$\widetilde{K}_{\text{th}} = a_{\text{th}} \Phi_{\text{th}} \tag{22}$$

$$\Phi_{\text{th}} = \left[n_{\lambda_r}^2 n_{\text{soi}} \;\; n_{\lambda_r} n_{\text{soi}} \;\; n_{\text{soi}} \;\; n_{\lambda_r}^2 \;\; n_{\lambda_r} \;\; n_{T_{\text{rc}}} \;\; \frac{1}{T_{\text{ivc}} - T_{\text{ivc}}^{\min}} \;\; 1 \right]^{\text{T}} \tag{23}$$

$$n_{\lambda_r} = \frac{\lambda_r - 0}{1 - 0}, \quad n_{\text{soi}} = \frac{\theta_{\text{soi}} - 280}{390 - 280}, \quad T_{\text{rc}} = \frac{T_{\text{rc}} - 600}{1000 - 600} \tag{24}$$

where θ_{soc}^* is the start of combustion timing to match the measured θ_{50}, p_{ivc} and T_{ivc} are the pressure and temperature at IVC, n_c is the polytropic compression exponent, λ_r and T_{rc} are the recompression AFR and temperature, and θ_{soi} is the fuel injection timing. Equations (19)–(22) convey that the Arrhenius threshold K_{th}^* to precisely match the measured θ_{50} is obtained by inverting the θ_{soc} to θ_{50} linear fit (20) and then running the Arrhenius integration up to the desired θ_{soc}^* with the estimated pressure and temperature. K_{th}^* then takes the place of the "measured" output that the model prediction $\widetilde{K}_{\text{th}}$ tries to approximate using a normalized parameterization that follows the same form as in Ref. [1] including an augmented term for T_{ivc}. The hyperbolic dependence on T_{ivc} is chosen to approximate the profile of the full Arrhenius correlation, which tends to have a nonlinearly increasing slope as T_{ivc} decreases and misfire conditions are approached. The $T_{\text{ivc}}^{\min}$ shift factor is chosen near the lower range of feasible T_{ivc} values to increase the sensitivity of the hyperbolic dependence in that region, but still outside the feasible T_{ivc} range to avoid dividing by zero. Note that the Arrhenius integration in Eq. (19) is evaluated using the look-up table method described in Ref. [1].

3 Experimental Results

The SI and HCCI parameter update methods described in Sec. 2 are augmented to the baseline SI–HCCI transition controller and implemented on the experimental engine from Ref. [1]. The experimental conditions are perturbed from those in Ref. [1] by use of a different fuel batch. Daily checkpoints indicate that this new fuel batch tends to increase the tendency toward engine knocking relative to the batch used in Ref. [1]. The performance of the baseline controller thus suffers in some experimental trials, though it will be shown that parameter adaptation is able to restore performance and even surpass the baseline results in Ref. [1] in most cases. As in Ref. [1], the responses of two of the four cylinders that elicit anomalous torque and AFR responses are omitted.

3.1 Successive Adaptations at One Operating Condition. The parameter adaptation is carried out in the simple case where successive SI–HCCI transitions are repeated at a single intermediate load operating condition of 2.4 bar NMEP at 2000 RPM with parameter updating active during all trials. A total of 16 SI–HCCI trials are run with the forgetting factor of the recursive least squares update tuned to an aggressive value of 0.94. This simplifies the experiments by hastening the adaptation process so that fewer adaptive SI–HCCI trials are required to observe the effects of the adaption at a single operating condition. The first experimental result compares SI–HCCI transition responses before and after the adaptive trials take place at constant operating conditions to illustrate the major effects of the adaptation. Figure 1 plots the responses before (left) and after (right) adaptation, where combustion inputs and outputs are shown in the upper and lower three rows, respectively. The θ_{sp} axis is adjusted for visibility in the SI phase; in the HCCI phase, θ_{sp} is placed after top dead center (aTDC). The displayed responses correspond to the first and second cylinders to enter HCCI, which are referred to as *H1* and *H2*, respectively, as in Ref. [1].

Observing the pre-adaptation responses in Fig. 1, it can be seen that minor errors are present in the SI phase of the transition associated with late θ_{50} for cylinder *H1* and slight reductions in NMEP for cylinder *H2*, though the peak torque deviation of 7% for one cycle is within expected tolerance. However, when the HCCI phase commences, the controller makes significant errors in advancing θ_{soi} on the 2–3 cycles following *HCCI 0*, which amplifies early combustion phasing on these cycles and contributes to reductions in NMEP. Additionally, the torque output of cylinder *H2* tends to be lower than *H1* for a given fuel quantity, so that the NMEP of this cylinder remains low for multiple cycles after entering HCCI. These errors are compensated by the internal model control (IMC) output feedback; however, several cycles must elapse before the errors are fully attenuated because the bandwidth of the controller cannot be arbitrarily high.

After the combustion model parameters are adapted, the problems displayed in the baseline controller responses are for a large part inherently attenuated by the model-based calculations. The θ_{sp} command for cylinder *H1* is advanced relative to *H2*, giving a

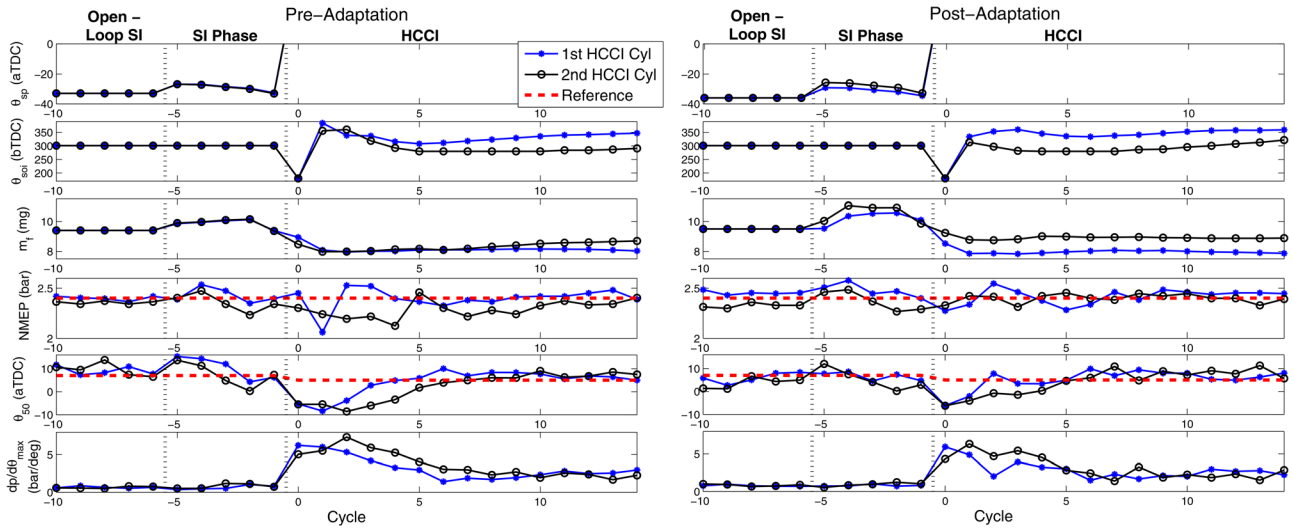

Fig. 1 SI–HCCI mode transitions before (left) and after (right) successive adaptations at an intermediate HCCI load operating condition. The first and second cylinders to enter HCCI are referred to as *H1* and *H2*, respectively.

θ_{50} response in SI that stays closer to the reference. The NMEP dip of cylinder *H2* in SI is kept to a lesser extent as well. In HCCI, the θ_{soi} command is not as advanced on the first few cycles following *HCCI 0*, most notably for cylinder *H2*. This causes θ_{50} to retard to its reference more readily after cycle *HCCI 0*, which has positive effects for the NMEP and $dp/d\theta_{\max}$ responses. Additionally, the m_f command for cylinder *H2* is increased relative to *H1*, which mitigates the excursion of cylinder *H2*'s NMEP below the reference that was observed in the pre-adaptation response. The adaptation thus enables errors to be immediately compensated by improving the model predictions, giving performance benefits during the cycles where direct output feedback would otherwise need time to adjust to cancel the errors. A last important comment is that the input trajectories for cylinders *H1* and *H2* are further apart than they are prior to adaptation, which is due to the fact that the baseline model is parameterized with a single set of coefficients. Differences in the cylinder's input trajectories in the baseline controller are thus only caused by corrective output feedback and differences in measured disturbance quantities (valve timing, intake pressure, etc.) between the cylinders, and the measured disturbances tend to be similar for both cylinders given that they are next to each other in firing order. The adaptation is carried out on a per cylinder basis, allowing each cylinder to be parameterized by its own set of coefficients and so inherently compensating for cylinder to cylinder variability.

For a more detailed view of how the parameter adaptation changes the controller response, Fig. 2 plots the input/output responses at the condition of Fig. 1 for several intermediate instances throughout the 16 adaptive trials. Separate plots are given for cylinder *H1* (left) and *H2* (right) because the adaptation occurs on a per cylinder basis. Moving from the dot-marked lines to the star-marked lines shows how a given trajectory changes with increasing adaptations. Observing the θ_{sp} and m_f input trajectories, a clear trend can be seen of advancing θ_{sp} on cylinder *H1* and increasing m_f on cylinder *H2* to compensate for the late SI θ_{50} of cylinder *H1* and lower NMEP of cylinder *H2*, respectively. The m_f command also increases slightly in SI for cylinder *H1*, though the change to the NMEP response is minor. Cylinder *H2*'s θ_{sp} command does not

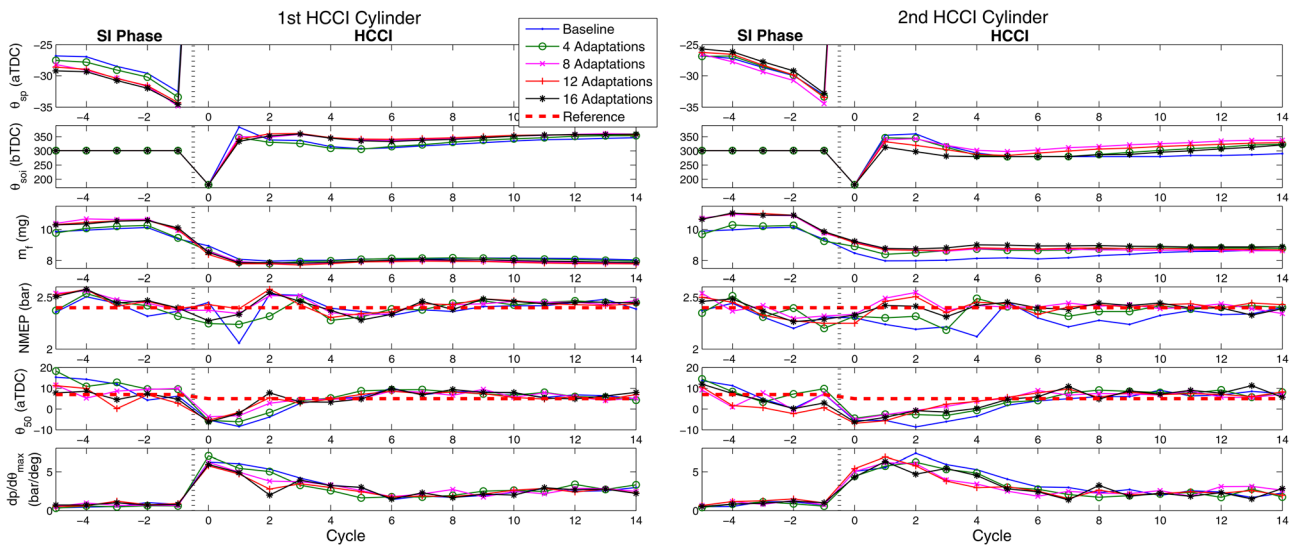

Fig. 2 Successive SI–HCCI mode transition trials at an intermediate HCCI load operating condition with adaptation active. The first and second cylinders to enter HCCI are referred to as *H1* and *H2*, respectively.

appear to have significant error as its variation with increasing adaptations seems mainly influenced by noise. Generally speaking, the θ_{sp} and m_f trajectories tend to converge within a small tolerance after eight adaptations.

The θ_{soi} trajectory, however, shows more significant variation as the adaptation progresses beyond eight trials, mainly in the first few cycles following *HCCI 0*. On cycle *HCCI 0* in particular, the adaptation unfortunately cannot help mitigate the early combustion phasing that occurs due to saturation of the θ_{soi} actuator at its maximum retard limit beyond which θ_{50} exhibits no sensitivity. It can be observed that the controller places θ_{soi} at this limit across all adaptive trials, because even in the unadapted case it recognizes that the high exhaust temperature carried over from cycle *SI-1* will lead to a very early combustion phasing. On the transient cycles following *HCCI 0*, however, the adaptation has a more significant effect. As θ_{50} tends to be early on these cycles, θ_{soi} continues to retard with increasing adaptive trials, most notably on cycle *HCCI 1* where the θ_{soi} retards by 17 deg for cylinder *H1* and 27 deg for cylinder *H2* between eight and 16 trials. After cycle *HCCI 1*, cylinder *H1*′s θ_{soi} command is actually later for the zero and four adaptation cases, which is most likely due to the IMC feedback's retarding θ_{soi} by a greater amount due to the earlier θ_{50} on cycle *HCCI 1* in these cases. The θ_{50} response of cylinder *H2* is slower to retard to the reference value than that of cylinder *H1*, which is reasonable given that this cylinder tends to have earlier combustion phasing and higher ringing amplitude in general. This promotes a more dramatic retarding effect on the θ_{soi} trajectory with increasing adaptations, to the point where after 16 adaptations cylinder *H2*'s θ_{soi} command is close to the nominal 280 deg before top dead center (bTDC) θ_{soi} saturation limit immediately after cycle *HCCI 0*. This gives a general trend of faster retarding θ_{50} and reduced pressure rise rates on the cycles following *HCCI 0*; however, even with the much later θ_{soi} at higher degrees of adaptation, cylinder *H2*′s θ_{50} still takes several more cycles to retard to the reference than for *H1* due to the cylinder to cylinder variability.

Despite that the SI–HCCI transition performance output trajectories become fairly consistent by the end of the 16 adaptive trials, it was found that the adapted model parameters did not in fact converge to steady-state values by the end of these trials. To investigate this outcome, a simulation study that considered a higher number of adaptive SI–HCCI trials was carried out. In the simulation study, the model of Ref. [16] was used to emulate the engine, and the controller model was initialized with parameter errors in its torque and combustion phasing calculations. SI–HCCI transitions were then iteratively simulated with adaptation active while observing changes in the controller parameters and SI–HCCI transition performance with increasing adaptations.

Figure 3 plots example parameter trajectories from the controller's HCCI torque and combustion phasing adaptive models to convey the parameter response over many repetitive adaptive trials. In the left column with the nominal least squares parameter update, it can be seen that the parameters experience large excursions after a high number of adaptive trials where data becomes repetitive. Using the simulation, the source of this divergence was traced to the estimator wind-up phenomenon [17]. In this phenomenon, the least squares basis function matrix P (see Eq. (4)) approaches singularity as the regressors that compose it become redundant.

Though estimator wind-up is less likely to be problematic in online implementation where the operating condition will continually vary and give less redundant data, it is advisable to modify the adaptive method to employ the directional forgetting algorithm as a safety precaution. The directional forgetting algorithm (see, e.g., Ref. [17]) prevents estimator wind-up by only forgetting data in the direction in which it is received, where direction refers to the orientation of an N-dimensional regressor vector in N-dimensional space. One implementation of directional forgetting [17] results in the modification of the P update expression (Eq. (4)) to

$$P^{-1}(m) = P^{-1}(m-1) + \left(1 + (\beta - 1) \times \frac{\Phi(m-1)^{\mathrm{T}} P^{-1}(m-1)\Phi(m-1)}{\left(\Phi(m-1)^{\mathrm{T}}\Phi(m-1)\right)^2}\right) \times \Phi(m-1)\Phi(m-1)^{\mathrm{T}} \quad (25)$$

where the update is now in terms of P^{-1}. When the adaptive simulation study was repeated using this directional forgetting update, parameter convergence was attained as is depicted in the right column of Fig. 3, and SI–HCCI transition performance did not deteriorate. Using the convergence criterion that a parameter remains within 0.1% of all future values on subsequent adaptive iterations, the θ_{soi} parameter in Fig. 3 attains convergence in 13 iterations and the m_f parameter attains convergence in 20 iterations. While the convergence rates are not exactly equal, they at least fall within a reasonable window of each other, i.e., it does not require an order of magnitude more iterations to converge some parameters than others. Note though that differences in the convergence rate between these parameters may be influenced by differences in the initialization of the P matrices for the θ_{50} and NMEP adaptive models. The final steady-state value is not equal to the true value, potentially due to a lack of persistent excitation after a high number of repetitive trials. Though the true parameters are not determined, the controller's performance still improves with adaptive trials relative to the initial parameter values, which is the main goal for the parameter adaptation. The simulation study thus suggests that if the parameter update algorithm is modified to include directional forgetting, the controller will retain the same improved and consistent performance observed after 16 experimental trials for an indefinite amount of trials.

3.2 Multiple Operating Conditions. The results of Sec. 3.1 show that the proposed parameter adaptation can yield significant improvements when applied at one operating condition. The effect of the adaptation on the controller response in differing operating conditions is now examined, in the limiting case where the adaptation is conditioned on data only from a single operating condition. That is, the controller parameters are adapted in successive SI–HCCI trials at a single condition, and then the controller is taken outside this condition to carry out SI–HCCI transitions without first being adapted at the altered conditions. This emulates the worst-case scenario where a driver's behavior tends to favor entry to HCCI in a narrow range of conditions so that the controller adapts mainly in that range, and then the controller is suddenly taken outside that range due to a change in driving pattern. The

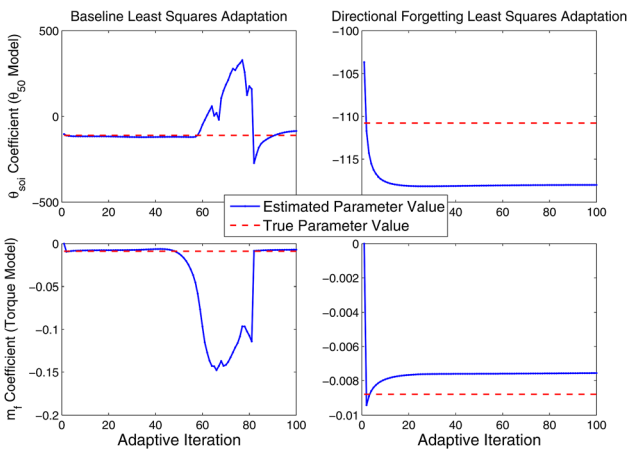

Fig. 3 Selected parameter trajectories from simulation of successive adaptive SI–HCCI trials at one operating condition to convey the divergence observed with the baseline least squares update law (left) and the prevention of such divergence using the directional forgetting least squares update law (right)

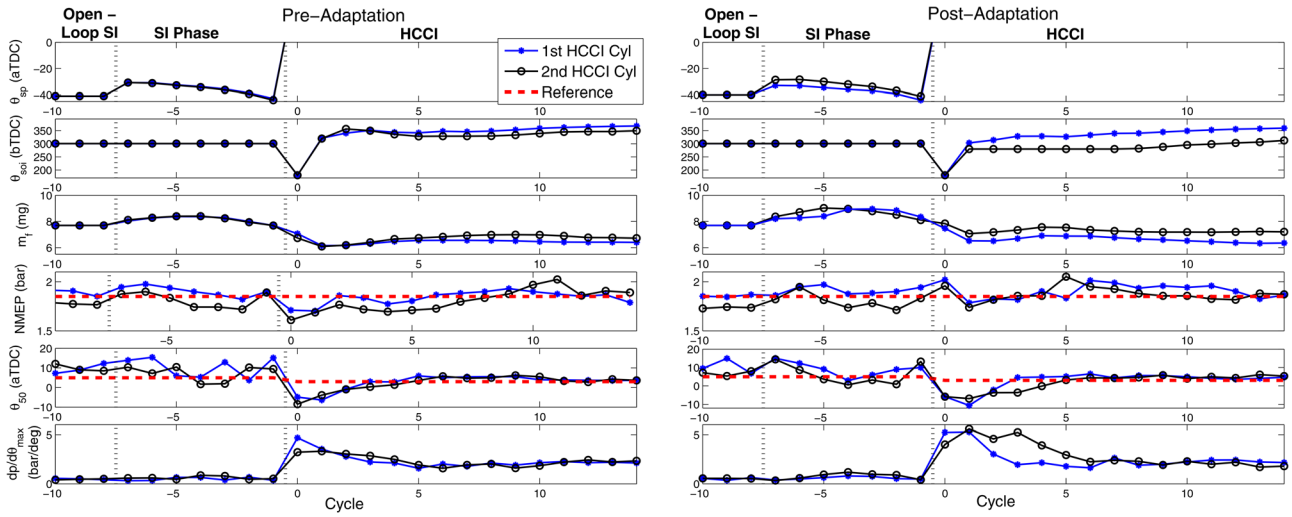

Fig. 4 SI–HCCI mode transitions near the low load HCCI limit before (left) and after (right) successive adaptations at the operating condition of Sec. 3.1

danger is that the adaptation will "overfit" to a narrow range of conditions so that performance will suffer when these conditions are exited. The operating condition for successive adaptations corresponds to that of Sec. 3.1, so that the postadaptation experimental results that follow are generated using parameter values taken at the end of the adaptive trials in Sec. 3.1.

The first set of experimental results considers varying load conditions for the SI–HCCI transition that span the HCCI load range of the experimental engine at 2000 RPM, similar to the low and high load conditions of Ref. [1]. As in Ref. [1], cylinder *H2* exhibited anomalous torque and AFR responses at the high load condition, wherein the torque could sporadically increase accompanied by a drop in AFR without a corresponding increase in the controller fuel command. These phenomena could last multiple cycles, leading to growing pressure rise rates and runaway knocking. Postexperimental engine teardown revealed a high in-cylinder deposit formation and leakage of oil past the intake valve guides on this cylinder, which may have contributed to this behavior. To prevent these deleterious effects from damaging the cylinder hardware, cylinder *H2* was configured to operate with a reduced fuel quantity that reduced its torque output below the reference at the high load condition, and so its response is omitted in this case.

Figures 4 and 5 plot the combustion responses with the baseline controller (left) and after adaptation (right) for the low load and high load cases, respectively. The general observation can be made from both figures that the NMEP response appears more favorable after adaptation in all cases. In the low load case, the adapted parameters induce a higher fuel mass for cylinder *H2* when HCCI is entered, which essentially eliminates the drop in NMEP seen in the baseline controller response for which the IMC feedback must compensate over multiple HCCI cycles. Note however that the higher fuel quantity commanded in the postadaptation case appears to contribute to θ_{50} values that are similar or even slightly earlier than the baseline case over the first few HCCI cycles. The postadaptation controller commands later θ_{soi} than the baseline controller during these cycles to the point of saturating the θ_{soi} command on cylinder *H2*; however, the effect on θ_{50} is not great enough to compensate for the higher fuel quantity and so higher $dp/d\theta_{\max}$ values result for the postadaptation controller. While the increased pressure rise rates are not of great concern because they do not exceed the preferred threshold of 6 bar/deg in this case, the example still shows that it is possible for the adaptation to cause some performance variables to suffer while others benefit in varying operating conditions. In the high load case, mainly positive results are seen comparing the pre- and post-

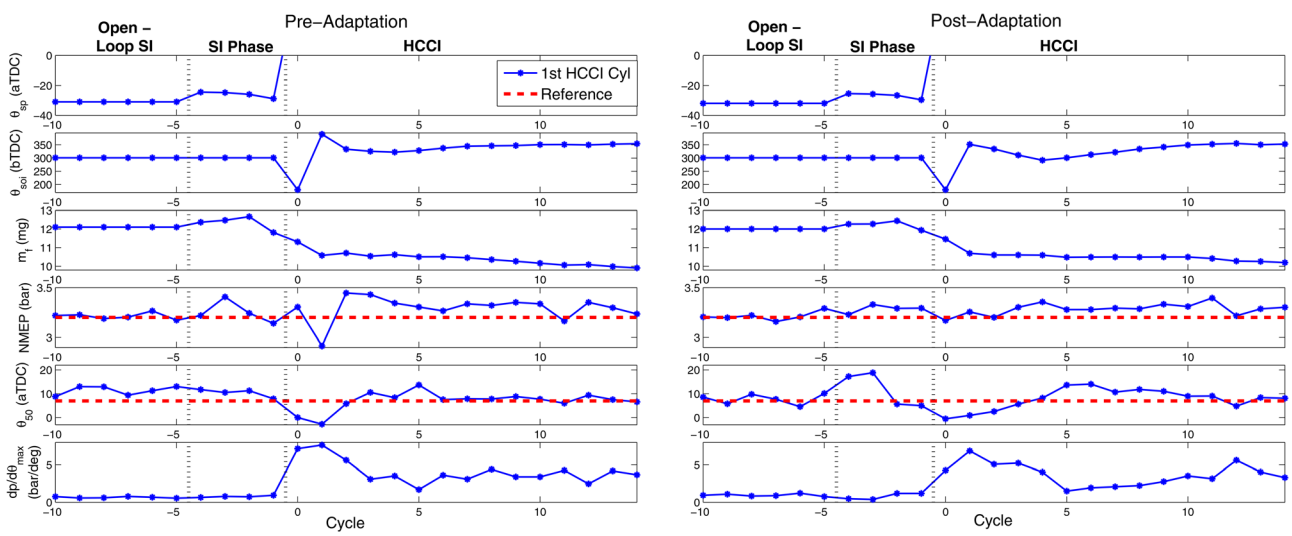

Fig. 5 SI–HCCI mode transitions near the high load HCCI limit before (left) and after (right) successive adaptations at the operating condition of Sec. 3.1

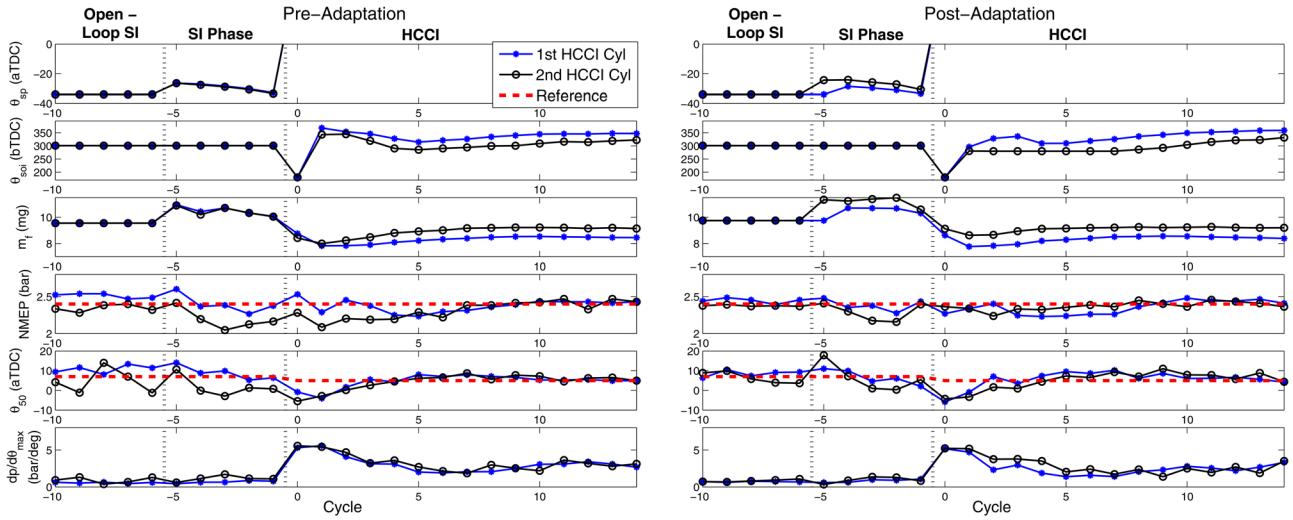

Fig. 6 SI–HCCI mode transitions with negative 250 RPM speed perturbation before (left) and after (right) successive adaptations at the operating condition of Sec. 3.1

adaptation responses, with the most notable benefit being the later θ_{soi} commanded on cycle *HCCI 1* in the postadaptation case. The later θ_{soi} yields a less advanced θ_{50} than in the baseline case, mitigating the torque reduction that results on cycle *HCCI 1* in the baseline case and giving lower $dp/d\theta_{max}$.

The second set of experimental results considers perturbations to the engine speed in a 500 RPM range about the nominally parameterized engine speed of 2000 RPM. Over this RPM range, the controller model has no speed dependent parameterization, with only physical dependencies on engine speed being present, such as conversion from air flow to charge mass. As with the high load case previously considered, cylinder *H2* began experiencing runaway knocking and unreasonable AFR/torque responses at the higher speed condition, and so its response is omitted in this case.

The low- and high-speed perturbed cases of 1750 RPM and 2250 RPM at the load condition of Sec. 3.1 are plotted in Figs. 6 and 7, respectively. Observation of these figures shows that both the baseline and adapted controller are able to handle the engine speed perturbation. However, comparison of the pre- and postadaptation outputs shows that again the responses in the adapted case are predominantly improved over the baseline. For both positive and negative speed perturbations, the postadaptation controller limits the maximum NMEP deviation to within 10%, a magnitude occurring over a period of only two cycles, while maintaining the pressure rise rate at less than the 6 bar/deg threshold for the entire transition. In the low-speed perturbed condition, the SI phase NMEP and θ_{50} responses stay closer to their references after adaptation, with the most notable effect being in the attenuation of the NMEP drop and early θ_{50} observed in cylinder *H2*'s baseline response. In the HCCI phase, again the drop in cylinder *H2*'s NMEP over the first several HCCI cycles is mitigated by the higher fuel command of the adapted controller. The θ_{soi} timing is also commanded later for both cylinders to aid in retarding θ_{50} to its reference, which has the greatest impact for cylinder *H1* on cycle *HCCI 1* where θ_{50} retards significantly further toward the reference than is seen with the baseline controller and gives a lower pressure rise rate. In the high-speed perturbed condition, the NMEP and θ_{50} responses stay within a similar vicinity of their reference for both the pre- and post-adaptation cases in the SI mode. However, when HCCI is entered, the adapted controller commands a later θ_{soi} than the baseline controller on cycle *HCCI 1*, which yields a later θ_{50} and keeps the NMEP reduction to a similar level despite the slightly lower fuel quantity. The θ_{50} of the adapted controller retards more quickly to its reference on the following several cycles as well, bringing pressure rise rates down faster.

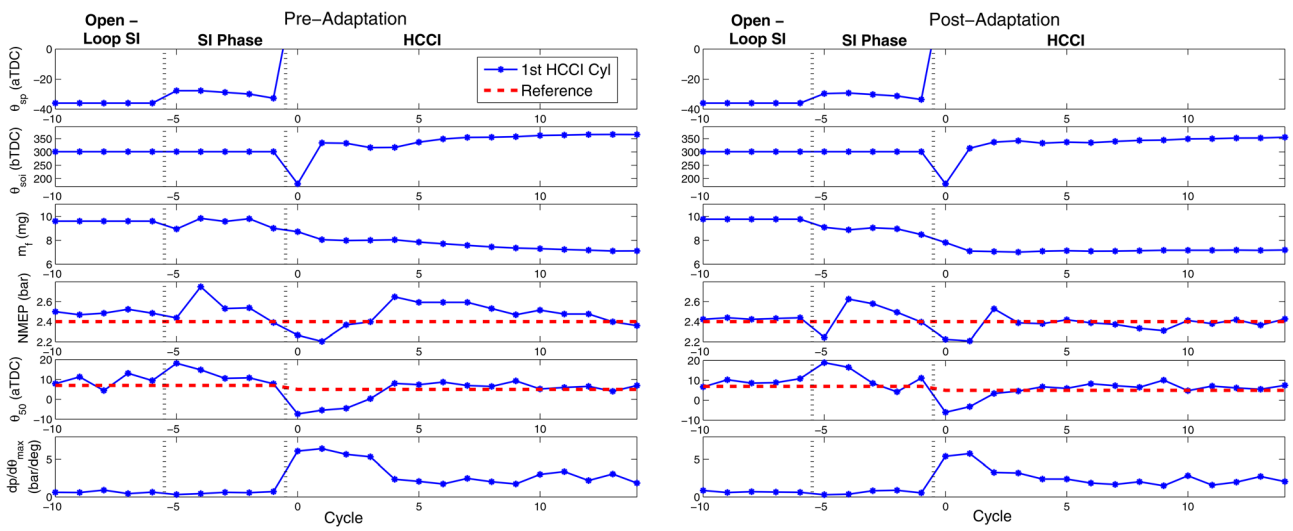

Fig. 7 SI–HCCI mode transitions with positive 250 RPM speed perturbation before (left) and after (right) successive adaptations at the operating condition of Sec. 3.1

4 Conclusion

A method to adapt the combustion model parameters of a previously developed model-based SI–HCCI transition controller [1] using online transient data has been proposed. The adaptation method employs linear least squares updating of the model's torque and combustion phasing correlations, which play a key role in the accuracy of the model-based control input commands. The adaptation method was implemented on an experimental engine and executed in real-time with online SI–HCCI transition data. Successive adaptive iterations at a single SI–HCCI transition condition yielded notable improvements in controller performance. The controller parameterization that was adapted only at a single operating condition was employed to carry out SI–HCCI transitions in other conditions to evaluate the sensitivity of the adaptive method to operating condition and discern any performance degradation caused by overfitting to a small set of conditions. Over a range of conditions spanning the experimental engine's HCCI load regime at 2000 RPM and a 500 RPM engine speed window at a fixed load, the results of the parameter adaptation on controller performance were predominantly positive, despite that the parameters were adapted only at a single operating condition. The controller validation over a 500 RPM range around a single parameterized speed suggests that the amount of speed dependent parameterization to cover the full HCCI speed range (typically a ~1500 RPM range) will be reasonable. One SI–HCCI transition case did exhibit worse responses for HCCI pressure rise rates with the adapted parameters in place, where pressure rise rates were increased beyond the baseline case in order to give better torque tracking. This example showed that it is possible for the adaptation to cause some degree of performance degradation in the response of some output variables. However, on the whole, the degradation observed was minor compared to the benefits of the adaptation, and the performance variable responses with the adapted parameters were preferable to those with the baseline controller in all cases. The results thus suggest that the proposed adaptive method can be an effective way to improve the performance of the model-based SI–HCCI transition control scheme of Ref. [1] and help it cope with engine aging, cylinder to cylinder variability, and modeling error in general.

Future work will cover a model-based feedback control method for the HCCI–SI direction of the mode transition. A further avenue for future work is to incorporate the effects of spark assist on auto-ignition into the control-oriented model and extend the model-based feedback control framework to cam phasing type SI/HCCI mode transitions and the spark-assisted compression ignition combustion mode.

Acknowledgment

This material is based upon work supported by the Department of Energy (National Energy Technology Laboratory) under Award No. DE-EE0003533. This work is performed as a part of the ACCESS project consortium (Robert Bosch LLC, AVL, Inc., Emitec, Inc., Stanford University, University of Michigan) under the direction of PI Hakan Yilmaz and Co-PI Oliver Miersch-Wiemers, Robert Bosch LLC.

References

[1] Gorzelic, P., Sterniak, J., and Stefanopoulou, A., 2017, "SI-HCCI Mode Transitions Without Open-Loop Sequence Scheduling: Control Architecture and Experimental Validation," ASME J. Dyn. Syst., Meas., Control, epub.
[2] Koopmans, L., Ström, H., Lundgren, S., Backlund, O., and Denbratt, I., 2003, "Demonstrating a SI-HCCI-SI Mode Change on a Volvo 5-Cylinder Electronic Valve Control Engine," SAE Paper No. 2003-01-0753.
[3] Santoso, H., Matthews, J., and Cheng, W., 2005, "Managing SI/HCCI Dual-Mode Engine Operation," SAE Paper No. 2005-01-0162.
[4] Zhang, Y., Xie, H., Zhou, N., Chen, T., and Zhao, H., 2007, "Study of SI-HCCI-SI Transition on a Port Fuel Injection Engine Equipped With 4VVAS," SAE Paper No. 2007-01-0199.
[5] Milovanovic, N., Blundell, D., Gedge, S., and Turner, J., 2005, "SI-HCCI-SI Mode Transition at Different Engine Operating Conditions," SAE Paper No. 2005-01-0156.
[6] Tian, G., Wang, Z., Ge, Q., Wang, J., and Shuai, S., 2007, "Control of a Spark Ignition Homogeneous Charge Compression Ignition Mode Transition on a Gasoline Direct Injection Engine," Proc. Inst. Mech. Eng., Part D, **221**(7), pp. 867–875.
[7] Cairns, A., and Blaxill, H., 2007, "The Effects of Two-Stage Cam Profile Switching and External EGR on SI-CAI Combustion Transitions," SAE Paper No. 2007-01-0187.
[8] Kalian, N., Zhao, H., and Qiao, J., 2008, "Investigation of Transition Between Spark Ignition and Controlled Auto-Ignition Combustion in a v6 Direct-Injection Engine With Cam Profile Switching," Proc. Inst. Mech. Eng., Part D, **222**(10), pp. 1911–1926.
[9] Wu, H., Collings, N., Regitz, S., Etheridge, J., and Kraft, M., 2010, "Experimental Investigation of a Control Method for SI-HCCI-SI Transition in a Multi-Cylinder Gasoline Engine," SAE Paper No. 2010-01-1245.
[10] Nier, T., Kulzer, A., and Karrelmeyer, R., 2012, "Analysis of the Combustion Mode Switch Between SI and Gasoline HCCI," SAE Paper No. 2012-01-1105.
[11] Kakuya, H., Yamaoka, S., Kumano, K., and Sato, S., 2008, "Investigation of a SI-HCCI Combustion Switching Control Method in a Multi-Cylinder Gasoline Engine," SAE Paper No. 2008-01-0792.
[12] Widd, A., Johansson, R., Borgqvist, P., Tunestål, P., and Johansson, B., 2011, "Investigating Mode Switch From SI to HCCI Using Early Intake Valve Closing and Negative Valve Overlap," SAE Paper No. 2011-01-1775.
[13] Yang, X., and Zhu, G., 2012, "SI and HCCI Combustion Mode Transition Control of an HCCI Capable SI Engine," IEEE Trans. Control Syst. Technol., **21**(5), pp. 1558–1569.
[14] Zhang, S., and Zhu, G., 2014, "Model-Based Mode Transition Control Between SI and HCCI Combustion," ASME Paper No. DSCC2014-6148.
[15] Ravi, N., Jagsch, M., Oudart, J., Chaturvedi, N., Cook, D., and Kojic, A., 2013, "Closed-Loop Control of SI-HCCI Mode Switch Using Fuel Injection Timing," ASME Paper No. DSCC2013-3785.
[16] Gorzelic, P., Shingne, P., Martz, J., Stefanopouou, A., Sterniak, J., and Jiang, L., 2016, "A Low-Order Adaptive Engine Model for SI-HCCI Mode Transition Control Applications With Cam Switching Strategies," Int. J. Eng. Res., **17**(4), pp. 451–468.
[17] Astrom, K., and Wittenmark, B., 1995, *Adaptive Control*, Addison-Wesley, Mineola, NY.
[18] Heywood, J., 1992, *Internal Combustion Engine Fundamentals*, McGraw-Hill, New York.
[19] Eriksson, L., and Andersson, I., 2002, "An Analytic Model for Cylinder Pressure in a Four Stroke SI Engine," SAE Paper No. 2002-01-0371.